Available online at www.sciencedirect.com
ScienceDirect
Trans. Nonferrous Met. Soc. China 29(2019) 143−156
Transactions of Nonferrous Metals Society of China
www.tnmsc.cn

High performance room temperature gas sensor based on novel morphology of zinc oxide nanostructures

Naila ZUBAIR, Khalida AKHTAR

National Center of Excellence in Physical Chemistry, University of Peshawar, Peshawar-25120, Khyber Pukhtoonkhwa, Pakistan

Received 9 February 2018; accepted 6 July 2018

Abstract: Zinc oxide uniform nanostructures with novel morphologies were synthesized through simple and fast ammonia based controlled precipitation method in aqueous media and in the absence of any additive. Selected batches of the synthesized solids were characterized by SEM, XRD, FTIR and TG/DTA. FTIR analysis revealed that the morphology of nanostructures had little effect on their IR spectral profile of the synthesized material. The as-prepared, calcined and commercial ZnO nanostructures (ZnO-AP, ZnO-Cal and ZnO-Com) were then employed as gas sensors for the detection of ammonia, acetone and ethanol. ZnO-AP and ZnO-Cal based sensors showed superior and reproducible performance towards 1×10^{-6} ammonia with gas response of 63.79% and 66.87% and response/recovery time of 13 and 3 s, respectively, at room temperature (29 °C). This was attributed to the unique morphology and remarkable uniformity in shape and size of the synthesized nanostructures. In contrast, the ZnO-Com based sensor did not respond to ammonia concentration less than 200×10^{-6}. In addition, ZnO-Cal showed high selectivity to ammonia as compared to acetone and ethanol at room temperature. Moreover, the lowest detection limit was 1×10^{-6}, which demonstrates excellent ammonia sensing characteristics of the synthesized ZnO.

Key words: zinc oxide nanostructures; gas sensor; sensitivity; response/recovery time

1 Introduction

Semiconductor metal oxide based gas sensors are among research projects addressing environmental concerns. The gas sensing properties of these sensors stem from the fact that the adsorption/desorption process of gases on metal oxide surfaces produces changes in their electrical resistance [1]. The magnitude of resistance variation is generally taken proportional to the amount of the reacting gases. In recent years, the use of ZnO in making gas sensors has captured the attention of many researchers because it is a good semiconductor with a band gap of 3.37 eV and its particles can be synthesized in a variety of different shapes and sizes [2,3]. In fact, the use of ZnO in making gas sensors can be traced back about 60 years. Since then researches have produced ZnO based gas sensors in different geometries for the detection of various gas types of environmental concern.

Ammonia gas, a toxic pollutant, is widely used and produced in many common industrial processes, such as food processing and fertilizers [4]. Ammonia leakage is always a danger in these processes and needs to be detected early on, before the onset of an accident. To address this concern, efforts have been made in the development of efficient, durable, and stable ammonia gas sensors [5,6]. Besides, volatile organic compounds (VOCs) especially acetone and ethanol are widely used both at laboratory scale as well as in industries. For instance, acetone is a common industrial solvent and is also generally accepted as one of the biomarkers, used for noninvasive diagnosis of type-1 diabetes [7]. Similarly ethanol has also a myriad of uses in industrial productions, as biofuel and in medicines as disinfectant, analgesic and sedative etc. However, due to high volatile and flammable nature at room temperature, their exposures increases to human body and can cause several adverse health effects [8,9]. Therefore, it is also essential to develop efficient and highly sensitive sensors which could detect trace amount of VOCs in residential as well as in industrial environments. However, it has generally been reported that a number of parameters, such as operating temperature, humidity, and interfering

Corresponding author: Khalida AKHTAR; E-mail: khalida_akhtar@yahoo.com
DOI: 10.1016/S1003-6326(18)64923-4

gases, affect the performance and sensitivity of the sensor. The sensor operation temperature is a matter of great concern [10] since it was noted in most of the previously mentioned published works that the semiconductor metal oxide based sensors operate in temperatures higher than ~200 °C, which limits their use in the low temperature environments. Notably, some researchers have made worthy attempts to produce ZnO based ammonia gas sensors at room temperature [11,12]. However, findings suggest that particle shape, size, and uniformity, among other variables, play a vital role in controlling the properties of the ZnO based gas sensors. As such, there exists ample room for further research in this important area, especially in tailoring the performance and sensitivity of the ZnO based gas sensors with ZnO powders composed of particles of different morphological features and chemical compositions.

ZnO particles have been prepared through various routes, such as the hydrothermal method [13], thermal evaporation process [14], chemical vapor deposition [15], electrophoretic deposition method [16], homogeneous precipitation method [17], and refluxing route [18]. In the present study, we have developed a simple, time effective, and economically feasible green method for the synthesis of uniform nanostructures of ZnO in different novel shapes and sizes that are most suitable for a wide range of applications.

The synthesized ZnO nanostructures and commercially available ZnO powder (Merck) were used for making gas sensors, which were then employed for the detection of ammonia, acetone, and ethanol vapors at room temperature as well as at high temperatures. Sensitivity of the synthesized ZnO nanostructures (as-prepared and calcined) was then compared with that of a commercial ZnO based sensor.

2 Experimental

2.1 Materials

Analytical reagent grade zinc nitrate (Sigma), ammonium hydroxide (Sigma), and ethylene glycol (Sigma) were employed as the starting chemicals and used without further purification. The stock and working solutions were made in deionized water and the suspected suspended impurities were removed from these solutions by filtration through a membrane filter.

2.2 Particles preparation

ZnO nanostructures were prepared through an ammonia-based controlled precipitation method. For this purpose, aqueous solutions, containing zinc nitrate (1.5−5 mol/L), ethylene glycol (1−15 mol/L), and ammonium hydroxide (1%−15%), were heated at 30−90 °C for 5−30 min. After the end of predetermined reaction time, the obtained precipitated solids were then isolated from the mother solutions by vacuum filtration through membrane filters and washed extensively with doubly distilled water and ethanol to ensure complete removal of any remnant of the precipitant solution. Finally, the powders were dried in air at room temperature and stored in a desiccator for characterization and application purposes.

2.3 Characterization

All the precipitated solids were inspected with a scanning electron microscope (SEM; JEOL, JSM−5910) at the accelerating voltage of 15 keV. Before each analysis, the powder samples were mounted on an aluminum stub with the help of a double-stick carbon conducting tape, and then sputtered with gold in a coater sputter (JEOL, JFC−1600, Auto Fine Coater). The crystalline nature of the selected batches of the precipitated particles was evaluated from the X-ray diffractograms, obtained from the X-ray diffractometer (XRD, JEOL JDX−3532) by using Cu K_α radiations. The applied voltage and current of the X-ray diffractometer were kept constant at 40 kV and 20 mA. In all cases, the samples were scanned in the 2θ range of 10°−80° with a step angle of 0.05°. The thermogravimetric/differential analyses of the desired powder samples were carried out by using a TGA/DTA analyzer (Diamond TG/DTA, Perkin Elmer). In all measurements, the samples were heated from 30 to 800 °C at a heating rate of 5 °C/min in the flow of air. The infrared spectroscopic analyses were performed with FTIR (Schimadzue, IR Prestige−21, FTIR−8400S) in the range of 400−4000 cm^{-1}. Similarly, a programmable furnace was used for the controlled calcination of the powder samples. The heating rate was kept at 5 °C/min, whereas the samples were cooled down to room temperature inside the furnace after switching it off.

2.4 Gas sensor fabrication and measurements

In this case, a uniform layer of the selected batches of ZnO nanostructures was pasted on the sensor platform (5 mm×5 mm alumina plate decorated with interdigitated gold electrodes) in the form of a thick layer and then dried at 300 °C for 2 h. After drying, both the electrodes were connected using a data acquisition system and the sensor plate was positioned in a reaction chamber of the gas sensing setup, fabricated for this purpose in the same manner as earlier for CuO nanospheroids [19]. The sensor plate was then exposed to ammonia (NH_3), ethanol (C_2H_5OH), and acetone ($(CH_3)_2CO$) in dynamic mode. In all cases, the flow rate of the gases was kept at 190 mL/min. The response of the sensor was registered in the form of its electrical

resistance. The acquired data were employed for calculation of sensitivity, response, and recovery times for the mentioned test gases. Electrical resistance of the same sensor plate was monitored in the same setup as a function of operating temperature in the range of 29−250 °C.

3 Results and discussion

3.1 Synthesis of zinc oxide (ZnO) nanostructures

ZnO nanostructures of novel morphologies were synthesized through ammonia-based controlled precipitation method. In this process, aqueous ammonia (15%−25%) was allowed to react with aqueous solutions of zinc nitrate (2−5 mol/L) at various temperatures for predetermined reaction time, which resulted in the precipitation of ZnO nanostructures. In fact, precipitation of zinc oxide particles takes place according to the following chain of reactions [20]:

$$Zn(NO_3)_2\cdot 6H_2O \rightarrow Zn^{2+} + 2NO_3^- + 6H_2O \quad (1)$$

$$Zn^{2+} + 2OH^- \rightarrow Zn(OH)_2 \rightarrow ZnO + H_2O \quad (2)$$

$$Zn^{2+} + 4OH^- \rightarrow Zn(OH)_4^{2-} \rightarrow ZnO + H_2O + 2OH^- \quad (3)$$

$$Zn^{2+} + 4NH_3 \rightarrow [Zn(NH_3)_4]^{2+} \quad (4)$$

$$[Zn(NH_3)_4]^{2+} + 2OH^- \rightarrow ZnO + 4NH_3 + H_2O \quad (5)$$

Preliminary trials indicated that in both cases, particle shape and size were significantly affected by the applied experimental parameters, especially aging time, reaction temperature, and reactants compositions. In order to obtain monodispersed nanostructures of ZnO of the same dimension and morphological features, extensive optimization of the mentioned reaction parameters was carried out in a systematic way. Figure 1

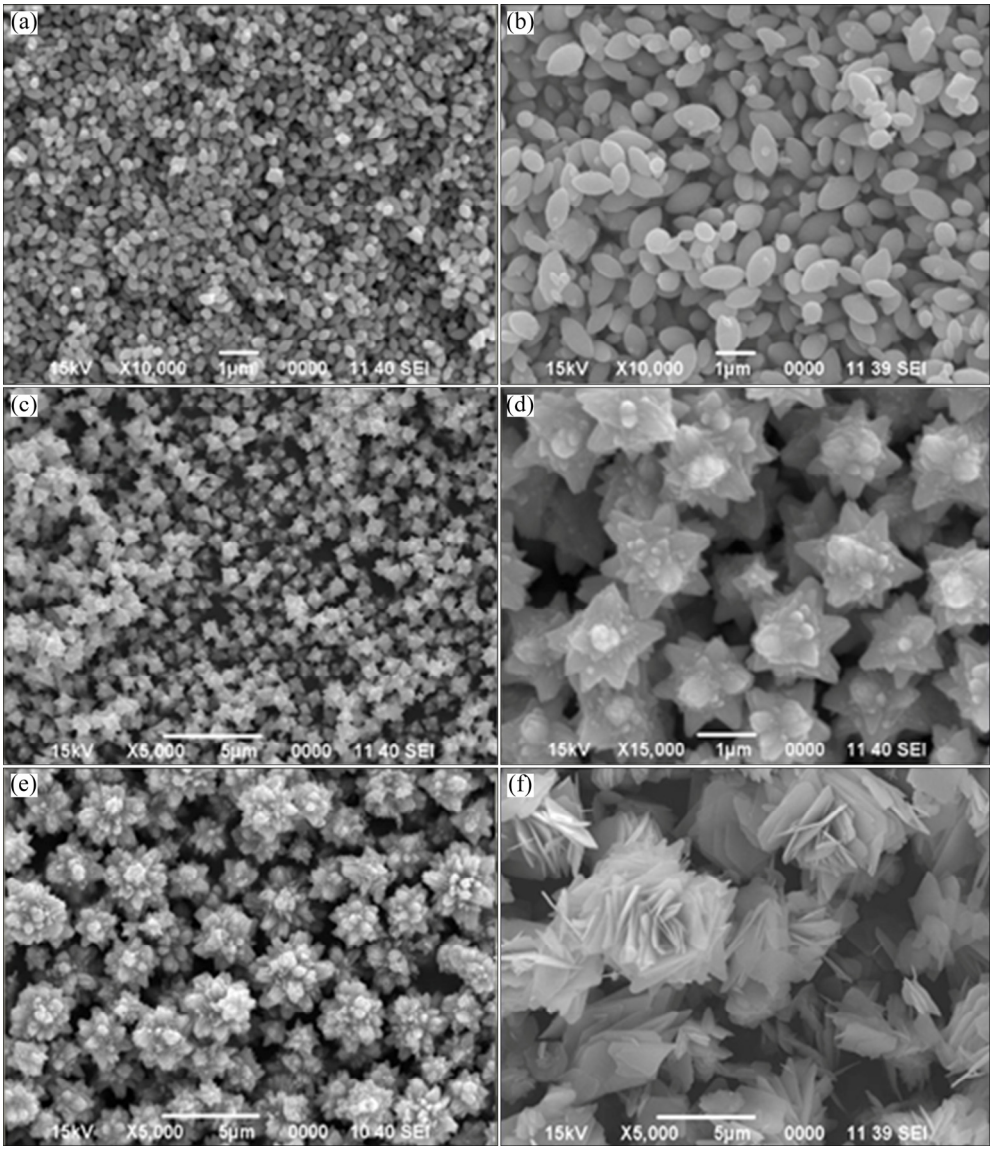

Fig. 1 SEM images of nanostructures precipitated from aqueous solutions containing zinc nitrate (1.5−5 mol/L), ethylene glycol (1−15 mol/L) and ammonium hydroxide (1%−15%) heated for 15 min: (a) 90 °C; (b) 80 °C; (c) 60 °C; (d) 50 °C; (e) 40 °C; (f) 30 °C

shows the SEM images of synthesized zinc oxide fine particles obtained from optimized amount of aqueous ammonia and zinc nitrate solution within 15 min, at 30−90 °C. From the SEM images, it can be seen that interesting and uniform morphologies appeared as the reaction temperature varied in the range of 30−90 °C. Figure 1(a) shows that powders precipitated at 90 °C are comprised of monodispersed ellipsoidal nanostructures. Since, the total reaction rate increases with increasing reaction temperature. Accordingly, high reaction temperature favors nucleation, while low temperature favors growth in the case of wet chemical synthesis of nanoparticles. In other words, at high temperature the nucleation rate constant k_1 would be larger, while the growth rate constant k_2 would get relatively smaller [21]. Ther ‘fore, it could be concluded that high temperature would result in the production of smaller size particles as compared to low temperature which would favor the formation of relatively larger size particles. It can be assumed that the nanoparticles could grow even better and larger at lower synthesis temperature, because lower temperature favors growth. As such, it was observed that the size of ellipsoidal nanostructures increased when the precipitation reaction was carried out at 80 °C, which is clear from the SEM image shown in Fig. 1(b). The nanostructures obtained at 60 °C are 3D, well dispersed flowers (Fig. 1(c)). It was indicated that the reaction temperature not only controls the particle size but also the growth orientation of the nanocrystals. Figure 1(d) shows that size of nanoflowers increased at 50 °C and continued to grow larger in size at 40 °C, as given in Fig. 1(e). Further decrease in reaction temperature (30 °C) favored the orientation of hierarchical flower-like nanostructures, as can be seen from Fig. 1(f).

It has been reported that initial nanocrystals nuclei form in the reactant solution which then grow up into nanopetals by Ostwald ripening. Due to the intrinsic anisotropic property of hexagonal crystalline structure, these nanopetals radially arrange and grow up along *c*-axis to decrease surface energy during the process and develop into 3D hierarchical flower-like nanostructures [22]. Such hierarchical flower-like ZnO structures have been reported previously by MENG et al [23] at relatively high temperature of 95 °C and longer reaction time of 6 h as compared to 30 °C in the present work.

3.2 Effect of morphology on FTIR-spectral profile of ZnO

The previously reported study [24] described the effect of particle morphology of iron oxide on their IR-profiles. It was of interest to evaluate the similar effects if any in case of ZnO nanostructures, was synthesized in the present study. FTIR spectra of the ZnO nanostructures of various morphologies, synthesized in this work (SEM, Fig. 1) were recorded and are displayed in Fig. 2. All the spectra were found to be composed of absorption bands at various locations (Table 1) due to different vibration modes of various chemical groups on the particle’s surface [25−31]. Inspection of Fig. 2 reveals that, despite significant variations in the particle morphologies, minor variations were observed in their IR profiles. For instance, some differences were noted in the frequencies of the OH^--bending vibrations. From this study, it may therefore be concluded that besides particle morphology, composition of the material should also be taken into account in interpreting their morphology-dependent FTIR spectra.

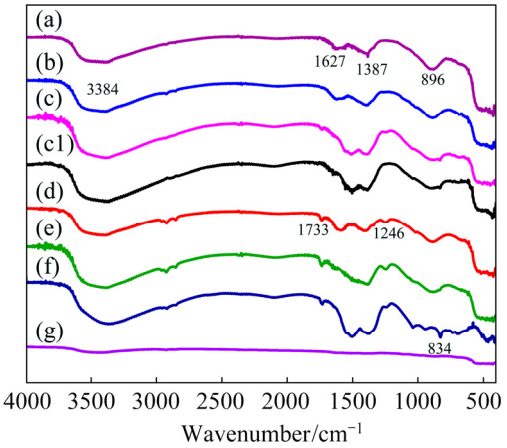

Fig. 2 Comparison of IR profiles of different ZnO morphologies shown in Figs. 1(a−f) (a−f), FTIR spectrum of calcined ZnO nanostructures (g), and FTIR spectrum of ZnO-AP after ammonia exposure and then flushed with air (c1)

Table 1 Wavenumber positions of chemical groups on solid

Band position/ cm^{-1}	Chemical group	Vibration mode	Reference
3384	OH^-	Stretching vibration	[25,26]
2096	OH^-	Stretching vibration	[27]
1733	C═O	Stretching vibration	[28]
1627, 1507	OH^-	Bending vibration	[25,29]
1381, 1387, 1246, 886, 834	NO_3^-	Stretching vibration	[26,30]
526−417	Zn—O	Stretching vibration	[31]

It is added that only the particles shown in Fig. 1(c) were selected for further characterization in this work because of the considerable uniformity in their particle shape and size.

Crystal structure as well as phase purity of the as-prepared ZnO nanostructures, presented in Fig. 1(c), were assessed through non-destructive powder X-ray diffraction (PXRD) technique and the obtained pattern

composed of sharp peaks at different 2θ values (Fig. 3(a)), which revealed that these nanostructures were crystallines in nature. All the intense and major diffraction peaks matched well with the standard diffraction data of ICDD No. 50664, as identified by means of JDX−3500 software. This suggests that the tested samples were nanocrystalline hexagonal ZnO with lattice parameters a=0.3249 nm and c=0.5205 nm [15,32]. Furthermore, the detected characteristic ZnO peaks positioned at 2θ values corresponded to the reflections from (100), (002), (101), (102), (110), (103) and (200) crystal planes [15]. No additional characteristic peaks for other phases were identified in the detection limit of X-ray diffraction, except the minor peak positioned at 2θ value of 16.93°, which is attributed to the remaining traces of $Zn(OH)_2$ formed during the course of formation of ZnO shown in Reaction (2) [33]. This distinctly confirmed that the as-prepared solid was well crystalline ZnO (zincite) [32,34]. Moreover, the present findings were in agreement with those reported by ZHANG et al [32], though they used sonochemical method for the preparation of ZnO nanostructures. This observation found that, for the present system, the synthesis route had negligible effect on its bulk characteristics.

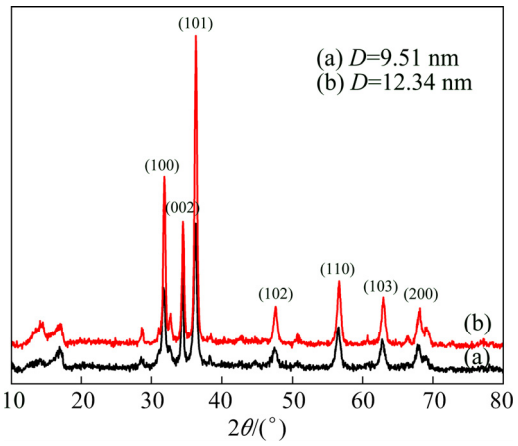

Fig. 3 XRD patterns of selected ZnO nanostrucrues shown in Fig. 1(c): (a) As-prepared; (b) After calcination at 800 °C

Similarly, a separate experiment was performed in which a known amount of the as-prepared ZnO sample was heated in a furnace at 800 °C for 2 h. As expected, SEM analysis (Fig. 4(a)) of the heat-treated solid showed that the observed mass losses brought obvious changes in the morphological features of the nanostructures.

The heat-treated solid was analyzed with XRD and the obtained pattern is given in Fig. 3(b). It can be noted that the XRD pattern was composed of very sharp peaks at the same positions, as observed in the XRD pattern of the as-prepared ZnO particles (XRD, Fig. 3(a)). This showed that heat treatment in the indicated temperature range did affect the crystalline structure of ZnO nanostructures. In addition, the data of the major peaks in both the XRD patterns were used for the calculations of crystallite size of as-prepared and calcined ZnO nanostructures by using the under-mentioned, yet well-known Debye Scherrer's equation [35]:

$$D=K\lambda/(\mathrm{FWHM}\cdot\cos\theta) \quad (6)$$

where D is the crystallite size of the particles (nm); K=0.9 (Scherrer constant); λ is the wavelength of X-rays used (nm); FWHM is the full width at half maximum of the major diffraction peak (rad); θ is the diffraction angle (rad).

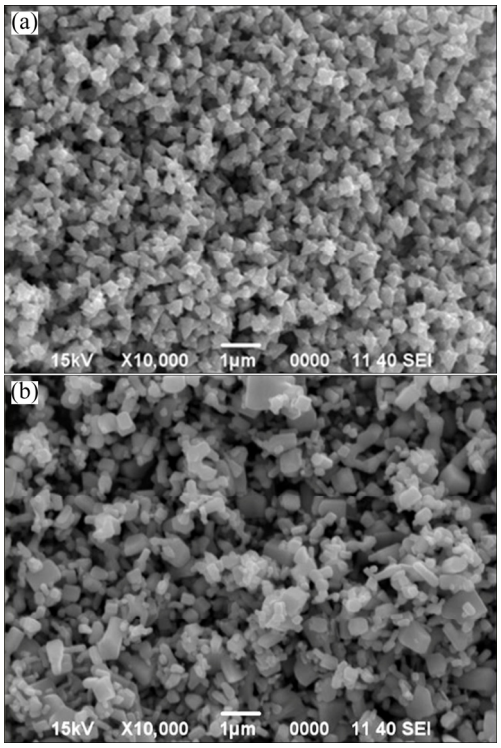

Fig. 4 SEM images of selected ZnO nanostructures shown in Fig. 1(c) after calcination at 800 °C (a), and commercial ZnO (b)

The surface groups of the heat-treated ZnO sample (SEM, Fig. 4(a)) were analyzed using an infrared spectroscopic technique and is shown in Fig. 2(g). It was found from the IR spectrum that the intensity of the band at 3449 cm^{-1} corresponded to the stretching vibrations of OH^- group of water molecules, adsorbed on the calcined particles due to their hygroscopic nature. The peaks observed at 2346, 1628, and 1518 cm^{-1} corresponded to the bending vibrations of the OH^- group and peak at 896 cm^{-1}, characteristic of NO_3^- group, lessened due to calcination at high temperature. A broad band in the range of 536−427 cm^{-1}, which is the characteristic of stretching vibration of Zn—O (metal−oxygen bonding), got intenser than the one observed in the FTIR spectrum (Fig. 2(c)) of the as-prepared sample. This showed that

heat treatment resulted in the purification of ZnO powder with respect to the remnant impurities.

3.3 Semiconducting properties

For fabrication of gas sensors, both as-prepared and calcined batches of synthesized ZnO (SEM, Fig. 1(c), Fig. 4(a)) and commercial ZnO (SEM, Fig. 4(b)) were employed which were designated as ZnO-AP, ZnO-Cal, ZnO-Com, respectively, in the further discussion.

Semiconducting properties of the three sensors (ZnO-AP, ZnO-Cal, ZnO-Com) were then monitored continuously in terms of electrical resistance against increasing temperature from 29 to 250 °C in the stream of dry air. Figures 5(a−c) depict the change in electrical resistance of these sensors as a function of temperature. As is evident from these figures, the electrical resistance of all three sensors decreased with the increase in temperature. This observation confirmed the semi-conducting nature of the three sensors [36]. In fact, on heating, the ZnO films, the charge carriers (i.e., electrons) gained enough energy to cross the energy barrier and jump from valence band to the conduction band and consequently decreased the electrical resistance of the sensor film.

In order to calculate the activation energy, the recorded resistance data were converted into respective conductance data and fitted into a linear form of Arrhenius equation (Eq. (7)) [19,36] and then ln σ was plotted against $1/T$, shown in insets of electrical resistance versus temperature plots of three sensors, respectively, of Fig. 5.

$$\ln \sigma=\ln \sigma_o-\Delta E_a/(kT) \quad (7)$$

where σ is the electrical conductance (S); σ_o is constant factor; ΔE_a is the activation energy (eV) required for electron transition from valence band to conduction band; K=8.617×10^{-5} eV/K (Boltzmann constant); T is the temperature (K).

The activation energy values estimated from the slopes of the straight lines for ZnO-AP, ZnO-Cal and ZnO-Com (given in inset of Fig. 5) were found to be 0.917, 0.902 and 1.30 eV, respectively (Table 2). The value of activation energy calculated for ZnO-AP and ZnO-Cal samples were very small as compared to that

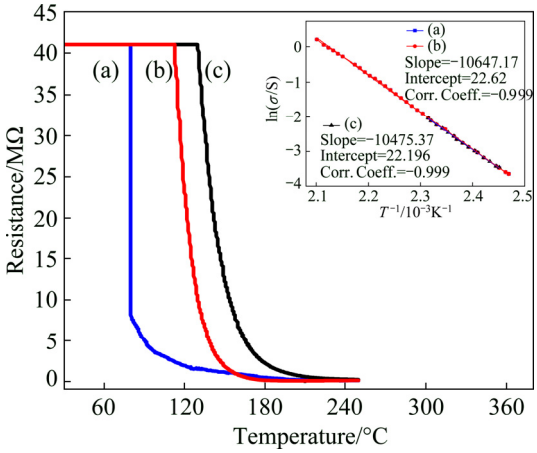

Fig. 5 Electrical resistance set against operating temperature for ZnO-AP (a), ZnO-Cal (b) and ZnO-Com (c) sensors along with ln σ versus $1/T$ plots in inset

for ZnO-Com, which was attributed to the distinguished uniformity in the morphology and good crystalline nature of the synthesized ZnO nanostructures [37]. The lower activation energy value of ZnO-Cal thus increased the semiconducting property of ZnO due to the increased crystalline nature and uniformity, which would possibly enhance the sensing performance of the semiconducting ZnO.

3.4 Gas sensing properties

After evaluating the electrical properties, the sensors were employed for the detection of ammonia, acetone and ethanol vapors under different operational conditions.

3.4.1 Ammonia sensing

Preliminary experiments revealed that each of the ZnO based sensors decreased in its electrical resistance when being exposed to ammonia gas. One of the possible mechanisms for ammonia sensing is that, in air ambient it is expected that the water molecules present on the sensor surface act as Bronsted acid sites while the incoming ammonia molecules act as Bronsted base and undergo the following acid base reaction [19]:

$$H_2O+NH_3 \rightarrow NH_4^+ +OH^- \quad (8)$$

$$NH_4^+ \rightarrow NH_3+H^+ \quad (9)$$

Table 2 Activation energies and maximum responses with corresponding optimum temperatures of selected ZnO-sensors towards ammonia, acetone and ethanol vapors

ZnO-sensor	Activation energy/eV	Ammonia vapor (200×10^{-6})		Acetone vapor (200×10^{-6})		Ethanol vapor (200×10^{-6})	
		Maximum response/%	Optimum temperature/°C	Maximum response/%	Optimum temperature/°C	Maximum response/%	Optimum temperature/°C
ZnO-AP	0.917	1025	109	1221	92	400	70
ZnO-Cal	0.902	1025	130	156	109	219	110
ZnO-Com	1.30	170	50	148	120	186	110

The NH_4^+ ions that result from the reaction in Eq. (8), hopped amongst the adjacent Bronsted acid sites, which created a temporary conducting film over the sensor surface and consequently caused a decrease in the electrical resistance of the sensor. Upon switching to dry air, the resistance of the sensor recovers to its original value. It has been suggested that the bonds involved between ammonia molecules and the sensor surface were weak physical forces, which were easily broken away when a stream of dry air was passed through. In addition, the other possible mechanism of semiconducting metal oxide is that in open air, the atmospheric oxygen gets adsorbed on its surface and engages a sufficient number of electrons of the conduction band. When it is exposed to the reducing gases, such as ammonia, the adsorbed oxygen is utilized in the oxidation of ammonia. In this process, the oxygen-trapped electrons are injected back into the conduction band, which results in a decrease in the electrical resistance of the ZnO sensor according to the following reaction routes [5,17]:

$$O_2(gas)+2e \rightarrow 2O^-(ads) \quad (10)$$

$$NH_3(gas) \rightarrow NH_3(ads) \quad (11)$$

$$NH_3(ads)+O^-(ads) \rightarrow [NH_2\cdot H\text{-}O]^-(ads) \quad (12)$$

$$2[NH_2\cdot H\text{-}O]^-(ads)+O^-(ads) \rightarrow N_2+3H_2O+3e \quad (13)$$

It is suggested that both the aforementioned mechanisms might be involved in the case of ammonia sensing, which was later be confirmed from the reproducible performance of the fabricated sensors towards ammonia gas, shown by the dynamic response curves.

3.4.1.1 Dynamic response

All three-sensor plates were exposed to dry air and a constant concentration of ammonia gas (200×10^{-6} in dry air) alternately for time intervals of 120 and 60 s at room temperature (29 °C). In this process, the variation in electrical resistance was continuously recorded through the data acquisition system connected to a computer. The electrical resistance data versus time, obtained under the described conditions, are presented in Fig. 6. Inspection of these curves revealed that for all three types of sensors, the electrical resistance decreased when the sensors were exposed to ammonia gas. The decrease in the electrical resistance was in fact caused by the release of electrons from the adsorbed oxygen to the conduction band of ZnO according to reaction mechanisms described in Eqs. (10)−(13). However, after the termination of the flow of ammonia gas and subsequent flushing with dry air, the sensors based on our synthesized ZnO nanostructures (as-prepared and calcined) retained their original resistance. In addition, the same type of behavior was observed in the remaining exposure cycles. The reproducibility in the performance of the sensor was ascribed to the uniformity in ZnO nanostructures, employed for the fabrication of these two sensors. In other words, the adsorption sites for the atmospheric oxygen, as well as ammonia molecules, were equally distributed on the sensor surface and the sensors responded in the same way in each of the exposure experiments. In addition, results revealed that, in the first instance, ammonia gas was physically adsorbed on the sensor surface with weak forces, which were easily overcome by the stream of dry air and were completely flushed away. To confirm the weak physical interaction of ammonia with sensor material and the resulting surface changes if any, a separate experiment was conducted in which the sensor material was exposed to ammonia gas and air, under the same ambient as described in Fig. 6.

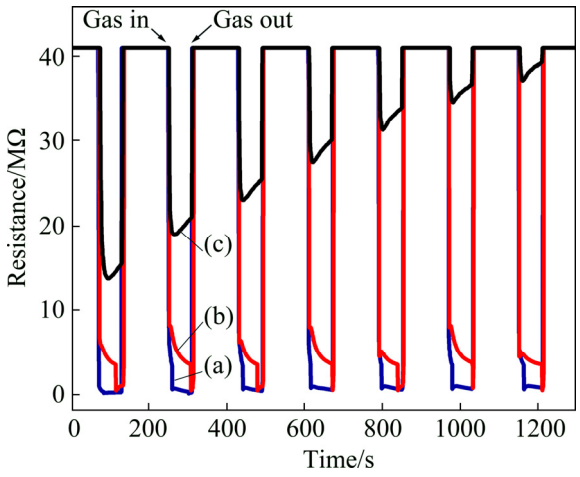

Fig. 6 Dynamic resistance response curves against time at room temperature (29 °C) to ammonia vapors (500×10^{-6}): (a) ZnO-Cal; (b) ZnO-AP; (c) ZnO-Com

The sensor material was then analyzed using FTIR and the recorded spectrum is given in Fig. 2(c1). It was found that the obtained spectrum matched well with the FTIR spectrum of the synthesized ZnO, shown in Fig. 2(c). It is worth mentioning that no extra peak appeared in the FTIR spectrum, which indicated that ammonia molecules get physically adsorbed and induced no surface changes in the sensor material.

In contrast, the nature of interaction of ammonia gas with the sensor made with commercial ZnO was different. As can be seen, each exposure of this sensor to ammonia gas led to the decrease in its response in a linear fashion. This showed that in each exposure to ammonia gas, the sensor surface probably retained the ammonia gas molecules by the chemisorption process and adsorption bonds were too strong enough to be broken down by the subsequent air flow. This resulted into permanent blockage of some of the adsorption sites on the sensor surface. The same process was repeated in

the rest of the exposure cycles, which ultimately made the sensor surface very much inactive for the detection of ammonia gas. It is worth mentioning that the performance of the synthesized ZnO based sensors with respect to sensitivity, response, and recovery time for ammonia sensing was much better (see Tables 2, 3) than our previously reported ZnO nanostructures, as well as those reported by other research groups. For instance, CHEN et al [5] investigated ZnO based ammonia sensing and recorded maximum sensor response of 81.6 s at 300 °C towards 1000×10^{-6} ammonia and reported 10×10^{-6} as the lower detection limit. PONNUSAMY and MADANAGURUSAMY [38] studied room temperature (30 °C) detection of ammonia and reported ~92 and ~111 s response/recovery time for the lowest ammonia concentration of 5×10^{-6}. VENKATESH et al [39] obtained 10% response to 100×10^{-6} ammonia with 49 and 14 s response/recovery time at room temperature. ANDRE et al [6] reported 4.5% for pure ZnO and 17% for 50% poly (styrene sulfonate) loaded ZnO with 51 and 160 s response/recovery time to 100×10^{-6} ammonia at room temperature.

It was therefore, concluded from this study, that the synthesized ZnO nanostructures possess great potential for the fabrication of ammonia gas sensors for such industrial environments, where ammonia is a matter of concern.

3.4.1.2 Effect of ammonia gas concentration

Following the aforementioned study, it was of interest to evaluate the response of three sensors towards different concentrations of ammonia gas in dry air. Hence, experiments were performed in which all three sensors were exposed to different concentrations of ammonia in dynamic mode at room temperature (29 °C). The obtained response curves are displayed in Fig. 7(a) for the ZnO-AP, ZnO-Cal, and ZnO-Com based sensors. As can be seen in Fig. 7(a), the amplitude of the resistance bands increased with the increase in concentration of ammonia gas, especially in the ZnO-AP and ZnO-Cal based sensors. In addition, these two sensors demonstrated good response towards 1×10^{-6} ammonia. In contrast, the ZnO-Com based sensor did not respond to an ammonia concentration less than 200×10^{-6}.

The recorded electrical resistance data in Fig. 7(a) were converted to the corresponding sensor response, using the relation for n-type metal oxide while detecting reducing gases [19,6]:

$$S=[(R_a-R_g)/R_a]\times100\% \quad (14)$$

where S is the sensor response (%), R_a is the sensor resistance in air (Ω) and R_g is the sensor resistance in the presence of ammonia gas (Ω).

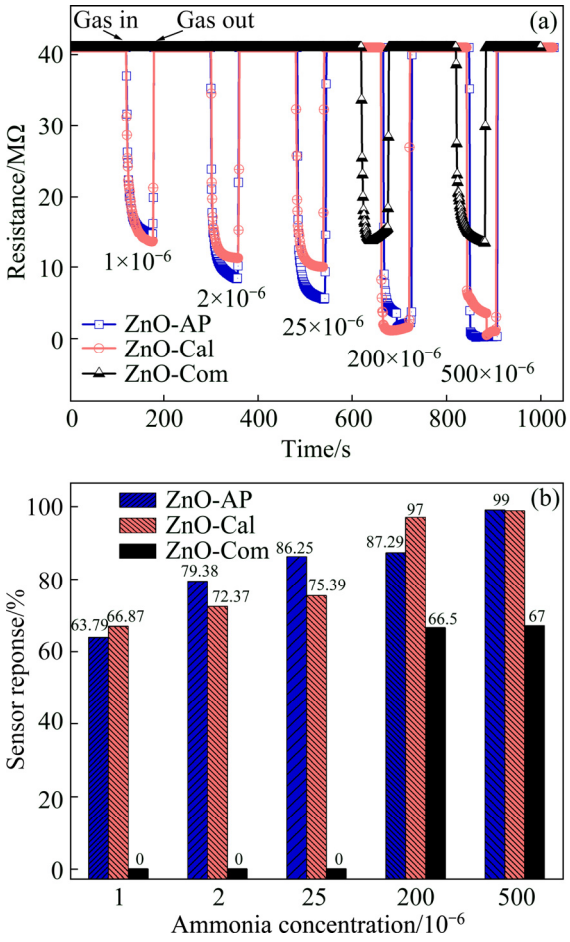

Fig. 7 Change in electrical resistance (a) and sensor response (b) against various concentrations of ammonia vapors (1×10^{-6}–500×10^{-6}) at room temperature (29 °C)

The corresponding response versus test gas concentration is plotted in Fig. 7(b). Similarly, the same data were also used for the estimation of response and recovery time for the three sensors under investigation and are included in Table 3. The response time is referred to the time taken by the sensor to attain 90% of its total resistance change when being exposed to ammonia gas, while the recovery time is the time taken by the sensor to regain 90% of the recovery from the maximum impact of the ammonia gas. Inspection of Table 3 shows that at the given concentration of ammonia gas, response of the ZnO-Com based sensor was poor as compared to ZnO-AP and ZnO-Cal based sensors. Similarly, response and recovery time turned out to be shorter for the latter sensors as compared to the ZnO-Com based sensor and the one we reported earlier [17]. These findings point to the fact that zinc oxide particles, synthesized in this work, were proven to be superior in performance for the detection of a wide range of ammonia gas concentration. Similarly, it was also revealed that the morphology of the nanostructure significantly affected the gas sensing properties of ZnO nanostructures.

Table 3 Sensor response with response and recovery time of ZnO-AP, ZnO-Cal and ZnO-Com sensors as function of ammonia concentration estimated at room temperature (29 °C)

NH_3-concentration/10^{-6}	Sensor response/%			Response time/s			Recovery time/s		
	ZnO-AP	ZnO-Cal	ZnO-Com	ZnO-AP	ZnO-Cal	ZnO-Com	ZnO-AP	ZnO-Cal	ZnO-Com
1	63.79	66.87	0	13	13	–	3	3	–
2	79.38	72.37	0	12	8	–	3	3	–
25	86.25	75.39	0	9	8	–	3	3	–
200	87.2	97	53.8	2	2	7	3	3	4
500	99	99	66	2	2	17	3	3	4

3.4.1.3 Effect of temperature on sensor response

Since gas response of metal oxide based sensors is generally affected by the ambient temperature [15,17,19], it is necessary to evaluate the effect of temperature on the performance of the three selected sensors towards the detection of ammonia. In this regard, the ammonia gas sensing experiments were performed by adjusting the sensor chamber temperature to the desired value. Results of the typical experiments are provided in Fig. 8. As can be seen, all three sensors exhibited different responses at different working temperatures. Sensors based on the synthesized ZnO nanostructures displayed excellent response in comparison to commercial ZnO over the entire temperature range deliberated. For instance, ZnO-AP and ZnO-Cal showed the same maximum response of ~90% at optimum temperatures of 109 and 130 °C, respectively (Table 2). In contrast, the ZnO-Com showed a response of ~40% at an optimum temperature of 50 °C. Additively, from Fig. 8, it is displayed that below and above optimum temperatures responses of the respective samples were on the lower side. This strange behavior of the sensor response with the operating temperature is controlled by atmospheric oxygen adsorption−desorption phenomenon at the surface of sensor film. In low temperature range, more oxygen molecules are adsorbed in the form of O_2^- and O^- ions, thus providing more active sites for reducing gases to react with and therefore release electrons into the conduction band. As a result, sensor response increased with increasing operating temperature up to the optimum limit. Since oxygen adsorption on film surface is an exothermic process [40], at temperature above optimum value, desorption of oxygen adsorbate anions starts, thereby decreasing the number of active sites for interaction with reducing gases and favors a decrease in response with further increase in operating temperature. The observed results indicated that the fabricated ZnO samples showed a response of almost more than double as compared to the one experienced by the commercial ZnO sample at the corresponding optimum temperatures. The excellent response of ~90% achieved for self-prepared samples at such a low working temperature has not yet been reported in the literature. The outstanding sensor responses of our prepared ZnO samples are ascribed to the unique morphology and remarkable uniformity in shape and size of synthesized nanostructures.

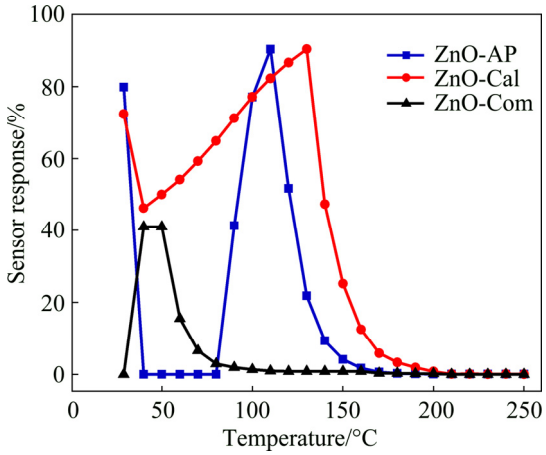

Fig. 8 Response of sensors at different operating temperatures towards ammonia vapors (200×10^{-6})

3.4.2 Acetone sensing

The same sensors (i.e., ZnO-AP, ZnO-Cal and ZnO-Com) were tested for the detection of acetone vapors. For this procedure, these sensors were independently exposed alternatively to air and a known concentration of acetone vapors at room temperature (29 °C) and their electrical resistance was continuously monitored at constant time intervals of 120 and 60 s, respectively, through computer-controlled system. All three sensors responded differently in terms of change in their electrical resistance in these cycles. Essentially, the change in electrical resistance of the ZnO based sensor, on contact with the reducing gas molecules, is caused by the interaction of the latter with the pre-adsorbed oxygen molecules on the sensor surface. As mentioned earlier, the adsorbed oxygen trap conduction band electrons from the semiconducting oxide surface are released back into the same band, when interacting with the reducing gas molecules. This type of acetone interaction may be described by the following reaction [41]:

$$CH_3COCH_3+8O^-(ads)\rightarrow 3H_2O+3CO_2+8e \quad (15)$$

It was observed that the ZnO-AP sensor showed no response towards the acetone vapors. This might be attributed to the possibility that a layer of adsorbed water was present on the sensor surface, which inhibited the approach of the acetone molecules to the active adsorption sites according to the aforementioned reaction (Eq. (15)). The inhibition of acetone molecules by the water molecules was obviously due to the non-miscibility of acetone molecules with adsorbed water layer. For instance, the Bronsted acid base reaction mentioned earlier in the case of ammonia sensing was not possible to occur, because of the small difference in pk_a values for water and acetone. Therefore, ZnO-AP showed no response to acetone at all. However, it was noted that the ZnO-Cal sensor responded to the first exposure of acetone (Fig. 9(a)) and then showed a decreasing trend in response in subsequent exposures. The gas response of the sensor was estimated from the data in Fig. 9 according to Eq. (14) and is given in inset of Fig. 9. It was shown that the sensor lost its response to a significant extent in the five exposures.

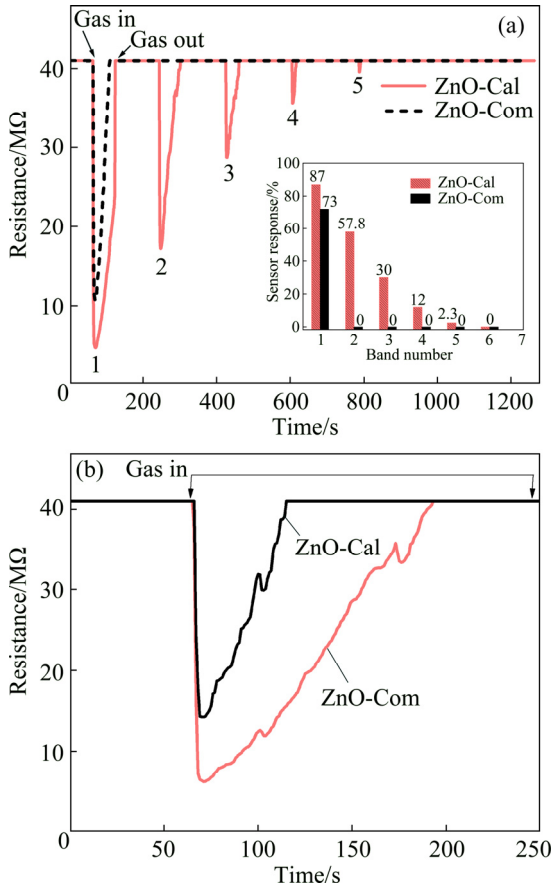

Fig. 9 Room temperature dynamic response of sensors towards head space vapors of acetone (200×10^{-6}) along with respective peak response vs band number shown in inset (a) and acetone chemisorption phenomenon at surface of sensors (b)

In order to account for the observed response of the ZnO-Cal sensor towards acetone, it appears that, in case of ZnO-Cal, the sensor surface was almost free from the adsorbed water, which can also be confirmed from FTIR spectrum of the calcined ZnO nanostructures (Fig. 2(g)). Therefore, the acetone molecules had access to the active sites on the sensor surface. Similarly, in each encounter, the acetone molecules were chemically adsorbed on the active sites and blocked them permanently. It might be due to the fact that acetone decomposition to carbon dioxide and water vapors according to Eq. (15) is favored at high working temperature [42]. Therefore, 29 °C operating temperature is low enough for complete decomposition of acetone to carbon dioxide and water vapors. As such, the sensor response was on the decline in the subsequent exposures to acetone vapors and finally the sensor surface became dead. This indicated the fact that unlike ammonia sensing, the acetone sensing by ZnO-Cal sensor is controlled only by the reaction given in Eq. (15) and no Bronted acid base reaction is involved. If it was so then the sensor would have shown reproducible performance instead of becoming dead.

Similarly, in case of the ZnO-Com sensor, electrical resistance decreased once acetone vapors were introduced into the chamber, holding the sensor and getting back to its original value when being flushed with dry air (Fig. 9(a)). However, in the subsequent cycles, the sensor did not respond anymore. It was observed that all available sites on the sensor surface were blocked, possibly, by the chemisorbed acetone molecules. These results suggest that the number of active sites on the ZnO-Com sensor was less than that on the ZnO-Cal sensor. In this regard, both ZnO-Cal and ZnO-Com sensors were exposed to a known amount of acetone vapors at room temperature. Figure 9(b) shows that electrical resistance of both the sensors first decreased due to available sites on sensor surfaces. After a certain interval of time, electrical resistance again increased and retained its original value even in the presence of acetone vapors. It is worth mentioning that the ZnO-Cal sensor was proven to have more vacant sites compared to the ZnO-Com sensor. Similarly, the response of ZnO-Com, as estimated by Eq. (14) for the single response band was ~73%, which was low compared to that calculated from the first response band of the ZnO-Cal sensor (87%). To our knowledge, no report is available that could describe the detection of headspace acetone vapors by pure ZnO based sensor at room temperature. Most of the research groups have used certain types of dopants to enhance the ZnO response toward acetone and at high operating temperatures rather than at room temperature [43,44].

3.4.3 Ethanol sensing

Additionally, gas sensing behavior of three sensors (i.e., ZnO-AP, ZnO-Cal and ZnO-Com) was evaluated

for the detection of ethanol vapors. Measurements were carried out at room temperature in which the desired sensors were exposed to plain dry air and headspace ethanol vapors alternatively for 120 and 60 s time intervals, respectively. Dynamic response curves in terms of change in electrical resistance of the sensor were measured during the aforementioned experiments. It was noted that the ZnO-AP sensor did not respond to the presence of ethanol in the sensor chamber, whereas ZnO-Cal and ZnO-Com responded to some extent as shown in Fig. 10. Analysis of these curves showed that the response of the ZnO-Cal sensor towards ethanol vapors was different from that of the ZnO-Com sensor, which could be attributed to the number of active reaction sites on the surfaces of these two sensors.

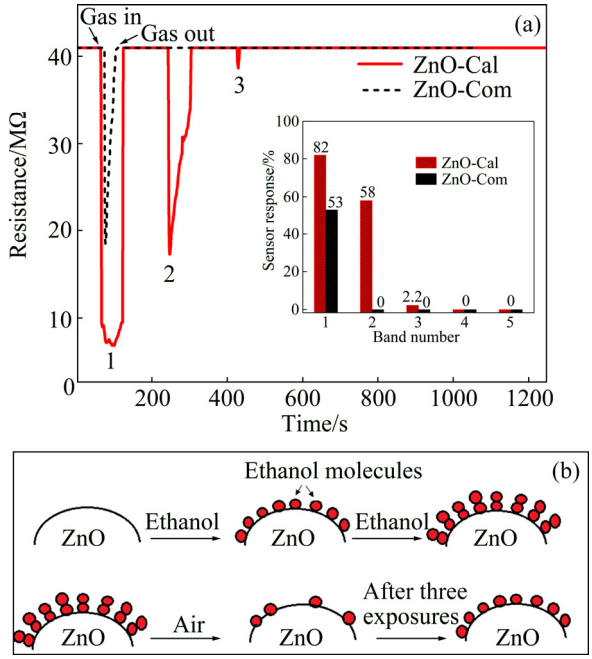

Fig. 10 Dynamic resistance response curves of sensors towards head space vapors of ethanol (200×10^{-6}) at room temperature (29 °C) along with respective peak response vs band number shown in inset (a) and schematic diagram for ethanol vapors adsorption and desorption on ZnO-Cal sensor film surface (b)

In fact, when ethanol vapors were introduced into the reaction chamber by holding the sensor through pressurized constant air flow, resistance of the sensors decreased immediately due to interaction between the already adsorbed oxygen on the sensor surface and upcoming ethanol molecules. This interaction caused the injection of electrons to the conduction band of the semiconducting ZnO and hence resulted into a decrease in the electrical resistance of the sensor according to the following reaction [42,45]:

$$CH_3CH_2OH(gas)+6O^-(ads)\rightarrow 2CO_2(gas)+3H_2O(gas)+6e \quad (16)$$

When the ethanol vapor flow was switched to plain dry air, the sensor should in principle retain its steady state electrical resistance due to the flushing away of the ethanol molecules from the sensor surface and subsequent occupancy of the same sites by the air oxygen. The latter process involved trapping of a sufficient number of conduction band electrons, which could be held responsible for bringing the electrical resistance of the sensor back to its steady state conditions. However, it was noted in Fig. 10(a) for ZnO-Cal that the intensity of resistance band showed a decreasing trend in the successive exposures to ethanol vapors, whereas in the case of ZnO-Com, only one resistance band was observed and showed no response in the rest of the exposures (Fig. 10(a)). Redox type interaction between the adsorbed oxygen ions and reducing gases is responsible for increase or decrease in sensor film resistance only. WANG et al [42] studied the interaction of ethanol with adsorb oxygen ions on film surface. They studied reactants of ethanol on the surface of respective sensor film through IR spectroscopy and reported that ethanol was decomposed to CO_2 and water in the temperature range of 40−420 °C through Eq. (16). Ethanol decomposition increased with increasing working temperature. In our experiments, the operating temperature (29 °C) might not be sufficient to completely decompose ethanol to CO_2 and water and therefore caused permanent blockage of the active sites. These observations indicated that the reaction mentioned in Eq. (16) was mostly chemical in nature. In the first exposure to ethanol vapors, most of the adsorption sites became occupied by the ethanol molecules, which could not be removed by the stream of air. This process of permanent blockage of the adsorption active sites went on in the subsequent exposures and all the sites were permanently blocked by the adsorbed ethanol molecules. The schematic diagram of the interaction of ethanol with sensor surface is shown in Fig. 10(b).

To determine the peak response for each resistance band in Fig. 10, the corresponding resistance data was converted into sensor response through Eq. (14) and the resulting plot is shown in the inset of Fig. 10(a). It is evident that the calculated peak response for the first band of the ZnO-Cal sensor curve was 82% at room temperature. Several investigations on ZnO based ethanol sensors showed that high working temperatures or certain types of dopants were desirable for the effective and fast response to ethanol vapors. Even Pd modified ZnO surface displayed only 10% response to a given concentration of ethanol at room temperature [46]. Moreover, CdO was also employed to improve ethanol sensing of ZnO at a high working temperature of 240 °C [47]. The ZnO-Cal response approached zero values after three successive cycles of ethanol exposures. It might be due to the surface saturation of the exposed

film by the chemisorbed ethanol molecules.

Similarly, the appearance of a single resistance band in the ethanol exposure experiment (Fig. 10(a)) revealed that the number of active sites on the ZnO-Com sensor surface were fewer than those of the ZnO-Cal sensor which were occupied by the ethanol molecules in a single exposure. Results revealed that in this case too, the interaction between the ethanol molecules and the sensor surface was chemical in nature, since the succeeding stream of air in the sensor chamber could not remove the adsorbed ethanol molecules from the surface. The calculated peak response (53%) for the observed single response band was much less than that observed for the ZnO-Cal sensor.

Furthermore, to account for the undetectable response of the ZnO-AP sensor towards ethanol, it appears that the surface of this sensor contained a layer of adsorbed water, inherited from the synthesis process. We believe that ethanol vapors in the ambient atmosphere could not replace the adsorbed water layer, possibly due to less surface affinity of ethanol molecules for the sensor surface as compared to adsorbed water molecules and thus showed no response. In addition, there is no Bronsted acid base reaction possibly because of nearly the same pk_a values of ethanol and water.

3.4.4 Selectivity

Selectivity of gas sensors is also an important parameter to evaluate the sensing performance. Gas sensors must have high selectivity towards the detection of gases. In the present case, ZnO-Cal showed response to all the three test vapors. To determine the selectivity, another experiment was conducted in which ZnO-Cal sensor was exposed to 1×10^{-6} of ammonia, acetone and ethanol vapors at room temperature (29 °C) under the same reaction conditions as presented in Fig. 6. The dynamic response of the sensor was recorded in terms of variation in resistance verses time continuously (Fig. 11).

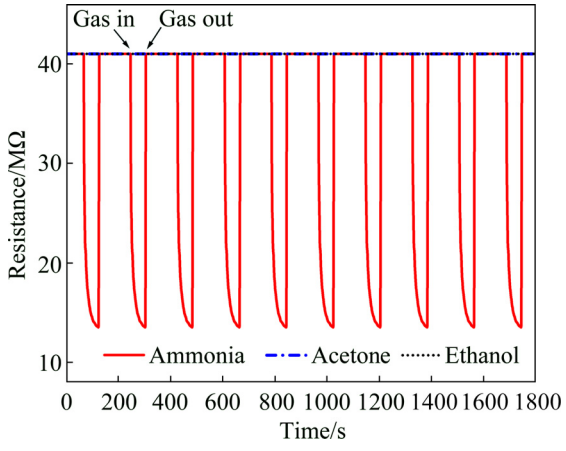

Fig. 11 Dynamic resistance response curves of ZnO-Cal towards same concentrations of ammonia, acetone, ethanol vapors (1×10^{-6}) at room temperature

The response curves in Fig. 11 illustrate that ZnO-Cal showed a reproducible response towards ammonia vapors. However, it showed no response towards acetone and ethanol vapors at such low concentration of 1×10^{-6}. Thus, the comparison of response curves suggests that the ZnO-Cal sensor was highly selective and sensitive to room temperature detection of ammonia, exposed at very low concentration (1×10^{-6}).

4 Conclusions

(1) Ammonia based controlled precipitation was proven to be a successful technique for the production of uniform nanostructures in different shapes and sizes with fast reaction time never reported earlier.

(2) XRD patterns showed that as-prepared ZnO nanostructures were composed of crystallines before being subjected to high temperature calcination.

(3) The superior and reproducible performance of ZnO-AP and ZnO-Cal based gas sensors towards the detection of ammonia gas as compared to ZnO-Com at room temperature can be attributed to the uniformity in particle size and shape of the synthesized nanostructures.

(4) The lowest detection limit (1×10^{-6} ammonia) demonstrated that synthesized ZnO nanostructures possess excellent sensing characteristics and great potential for the fabrication of ammonia gas sensor for such industrial environments, where ammonia is a matter of concern for the industrial workers.

(5) ZnO-Cal was highly selective towards room temperature detection of ammonia as compared to acetone and ethanol.

Acknowledgments

We are thankful to the National Center of Excellence in Physical Chemistry, University of Peshawar, Khyber Pakhtoonkhwa, Pakistan for facilitating this work.

References

[1] PRABAKARAN S, RAYAPPAN J B B. Gas sensing mechanism of metal oxides: The role of ambient atmosphere, type of semiconductor and gases—A review [J]. Science Jet, 2015, 4: 126(1−18).

[2] WU Shui-sheng, JIA Qing-ming, SUN Yan-lin, SHAN Shao-yun, JIANG Li-hong, WANG Ya-ming. Microwave-hydrothermal preparation of flower-like ZnO microstructure and its photocatalytic activity [J]. Transactions of Nonferrous Metals Society China, 2012, 22: 2465−2470.

[3] YANG Le-jiao, QIU De-liang, YU Fei, CHEN Shou-gang, YIN Yan-sheng. 3D flowerlike ZnO micro-nanostructures via site-specific second nucleation in the zinc–ethylenediamine–hexamethylenetetramine tertiary system [J]. Material Science in Semiconductor Processing, 2011, 14: 193−198.

[4] PATIL L A, SONAWANE L S, PATIL D G. Room temperature ammonia gas sensing using MnO_2-modified ZnO thick film resistors [J]. Journal of Modern Physics, 2011, 2: 1215−1221.

[5] CHEN Tai-You, CHEN Huey-Ing, HSU Chi-Shiang, HUANG Chien-Chang, WU Jian-Sheng, CHOU Po-Cheng, LIU Wen-Chau. Characteristics of ZnO nanorods-based ammonia gas sensors with a cross-linked configuration [J]. Sensors and Actuators B, 2015, 221: 491−498.

[6] ANDRE R S, KWAK D, DONG Qiu-chen, ZHONG Wei, CORREA D S, MATTOSO L H C, LEI Yu. Sensitive and selective NH_3 monitoring at room temperature using ZnO ceramic nanofibers decorated with poly(styrene sulfonate) [J]. Sensors, 2018, 18: 1058(1−13).

[7] MENG Fan-li, HOU Nan-nan, JIN Zhen, SUN Bai, LI Wen-qing, XIAO Xiang-heng, WANG Chen, LI Min-qiang, LIU Jin-huai. Sub-ppb detection of acetone using Au-modified flower-like hierarchical ZnO structures [J]. Sensors and Actuators B, 2015, 219: 209−217.

[8] MENG Fan-li, ZHENG Han-xiong, CHANG Yuan-long, ZHAO Yong, LI Min-qiang, WANG Chen, SUN Yu-feng, LIU Jin-huai. One-step synthesis of Au/SnO_2/RGO nanocomposites and their VOC sensing properties [J]. IEEE Transactions on Nanotechnology, 2018, 17: 212−219.

[9] SONG Young Geun, SHIM Young-Seok, KIM Sangtae, HAN Soo Deok, MOON Hi Gyu, NOH Myoung Sub, LEE Kwangjae, LEE Hae Ryong, KIM Jin-Sang, JU Byeong-Kwon, KANG Chong-Yun. Downsizing gas sensors based on semiconducting metal oxide: Effects of electrodes on gas sensing properties [J]. Sensors and Actuators B, 2017, 248: 949−956.

[10] WEI Ang, WANG Zhao, LIU Hua-pan, LI Wei-wei, XIONG Lie, DONG Xiao-chen, HUANG Wei. Room-temperature NH_3 gas sensor based on hydrothermally grown ZnO nanorods [J]. Chinese Physics Letters, 2011, 28: 1−4.

[11] SAROCH M, SRIVASTAWA S, FINK D. CHANDRA A. Room temperature ammonia gas sensing using mixed conductor based TEMPOS structures [J]. Sensors, 2008, 8: 6355−6377.

[12] BHASKER R V, NIMAL A T, PARMAR Y, SHARMA M U, SREENIVAS K. GUPTA V. Cross-sensitivity and selectivity studies on ZnO surface acoustic wave ammonia sensor [J]. Sensors and Actuators B, 2010, 147: 517−524.

[13] ZENG Yi, LOU Zheng, WANG Li-li, ZOU Bo, ZHANG Tong, ZHENG Wei-tao, ZOU Guan-tian. Enhanced ammonia sensing performances of Pd-sensitized flowerlike ZnO nanostructure [J]. Sensors and Actuators B, 2011, 156: 395−400.

[14] LV H, SANG D D, LI H D, DU X B, LI D M, ZOU G T. Thermal evaporation synthesis and properties of ZnO nano/microstructures using carbon group elements as the reducing agents [J]. Nanoscale Research Letters, 2010, 5: 620−624.

[15] ZHANG Jian-jiao, GUO Er-jun, WANG Li-ping, YUE Hong-yan, CAO Guo-jian, SONG Liang. Effect of annealing treatment on morphologies and gas sensing properties of ZnO nanorods [J]. Transactions of Nonferrous Metals Society of China, 2014, 24: 736−742.

[16] PU Xi-peng, ZHANG De-feng, YI Xiu-jie, SHAO Xin, LI Wen-zhi, SUN Ming-yan, LI Lei, QIAN Xian-hua. Rapid chemical synthesis and optical properties of ZnO ellipsoidal nanostructures [J]. Advanced Powder Technology, 2010, 21: 344−349.

[17] HAQ I U, AZAD A M. Experimental artifacts for morphological tweaking of chemical sensor materials: Studies on ZnO [J]. Sensors, 2012, 12: 8259−8277.

[18] ZHANG Jing-wei, WANG Wei, ZHU Peng-li, CHEN Jian-min, ZHANG Zhi-jun, WU Zhi-shen. Synthesis of small diameter ZnO nanorods via refluxing route in alcohol–water mixing solution containing zinc salt and urea [J]. Materials Letters, 2007, 61: 592−594.

[19] AKHTAR K, HAQ I U, MALOOK K. Gas sensing properties of semiconducting-copper oxide nanospheroids [J]. Powder Technology, 2015, 283: 505−511.

[20] HEIDARI A, YOUNESI H. Controllable synthesis of flower-like ZnO nanostructure with hydrothermal method [J]. IJE Transactions B: Applications, 2009, 22: 283−290.

[21] LIU Hong-yu, ZHANG Huan, WANG Jie, WEI Jun-fu. Effect of temperature on the size of biosynthesized silver nanoparticle: Deep insight into microscopic kinetics analysis [J]. Arabian Journal of Chemistry, 2017. https://doi.org/10.1016/j.arabjc.2017.09.004.

[22] MENG Fan-li, ZHENG Han-xiong, SUN Yu-feng, LI Min-qiang, LIU Jin-huai. Trimethylamine sensors based on Au-modified hierarchical porous single-crystalline ZnO nanosheets [J]. Sensors, 2017, 17: 1−13.

[23] MENG Fan-li, HOU Nan-nan, GE Sheng, SUN Bai, JIN Zhen, SHEN Wei, KONG Ling-tao, GUO Zheng, SUN Yu-feng, WU Hao, WANG Chen, LI Min-qiang. Flower-like hierarchical structures consisting of porous single-crystalline ZnO nanosheets and their gas sensing properties to volatile organic compounds (VOCs) [J]. Journal of Alloys and Compounds, 2015, 626: 124−130.

[24] WANG Yin-sheng, MURAMATSU A, SUGIMOTO T. FTIR analysis of well-defined Fe_2O_3 particles [J]. Colloids and Surfaces A: Physicochemical Engineering Aspects, 1998, 134: 281−297.

[25] ANAS S, MUKUNDAN P, SANOJ A M, MANGALARAJ V R. Synthesis of ZnO based nanopowders via a non-hydrolytic sol gel technique and their densification behavior and varistor properties [J]. Processing and Application of Ceramics, 2010, 4: 7−14.

[26] UMAR A, RAHMAN M M, AL-HAJRY A, HAHN Y B. Highly-sensitive cholesterol biosensor based on well-crystallized flower-shaped ZnO nanostructures [J]. Talanta, 2009, 78: 284−289.

[27] SARASWATHI M, CLAUDE A, DEVI K N, SEVVANTHI P. Growth of zinc oxide crystals by accelerated evaporation technique from supersaturated solutions [J]. International Journal of ChemTech Research, 2012, 4: 1343−1349.

[28] KHAN Y, DURRANI S K, MEHMOOD M, AHMAD J, KHAN M R, FIRDOUS S. Low temperature synthesis of fluorescent ZnO nanoparticles [J]. Applied Surface Science, 2010, 257: 1756−1761.

[29] CHANDRAPPA K G, VENKATESHA T V, VATHSALA K, SHIVAKUMARA C. A hybrid electrochemical–thermal method for the preparation of large ZnO nanoparticles [J]. Journal of Nanoparticle Research, 2010, 12: 2667−2678.

[30] WAHAB Rizwan, KIM Young-Soon, SHIN Hyung-Shik. Synthesis, characterization and effect of pH variation on zinc oxide nanostructures [J]. Materials Transactions, 2009, 50: 2092−2097.

[31] JEGAN A, RAMASUBBU A, KARUNAKARAN K, VASANTHKUMAR S. Synthesis and characterization of zinc oxide–agar nanocomposite [J]. International Journal of Nano Dimension, 2012, 2: 171−176.

[32] ZHANG Shao-Lin, BYUN Hyung-Gi, LIM Jeong-Ok, HUH Jeung-Soo, LEE Wooyoung. Controlled synthesis of ZnO nanostructures for sub-ppm-level VOC detection [J]. IEEE Sensors Journal, 2012, 12: 3149−3155.

[33] KUO Chia-Liang, WANG Cheng-Li, KO Horng-Huey, HWANG Weng-Sing, CHANG Kuo-Meng, LI Wang-Long, HUANG Hong-Hsin, CHANG Yen-Hwei, WANG Moo-Chin. Synthesis of zinc oxide nanocrystalline powders for cosmetic applications [J]. Ceramics International, 2010, 36: 693−698.

[34] BOZ I, KALUZA S, BOROGLU M S, MUHLER M. Synthesis of high surface area ZnO powder by continuous precipitation [J]. Materials Research Bulletin, 2012, 47: 1185−1190.

[35] SINGH A K. Synthesis, characterization, electrical and sensing properties of ZnO nanoparticles [J]. Advanced Powder Technology, 2010, 21: 609−613.

[36] GHADERI A, ELAHI S M, SOLAYMANI S, NASERI M, AHMADIRAD M, BAHRAMI S, KHALILI A E. Thickness dependence of the structural and electrical properties of ZnO

thermal-evaporated thin films [J]. Pramana–Journal of Physics, 2011, 77: 1171−1178.

[37] BEDI R K, SINGH I. Room-temperature ammonia sensor based on cationic surfactant-assisted nanocrystalline CuO [J]. ACS Applied Materials & Interfaces, 2010, 2: 1361−1368.

[38] PONNUSAMY D, MADANAGURUSAMY S. Nanostructured ZnO films for room temperature ammonia sensing [J]. Journal of Electronic Materials, 2014, 43: 3211−3216.

[39] VENKATESH P S, DHARMARAJ P, PURUSHOTHAMAN V, RAMAKRISHNAN V, JEGANATHAN K. Point defects assisted NH3 gas sensing properties in ZnO nanostructures [J]. Sensors and Actuators B, 2015, 212: 10−17.

[40] CHANG Shoou Jin, WENG Wen Yin, HSU Cheng Liang, HSUEH Ting Jen. High sensitivity of a ZnO nanowire-based ammonia gas sensor with Pt nano-particles [J]. Nano Communication Networks, 2010, 1: 283−288.

[41] BHOWMIK B, HAZARA A, DUTTA K, BHATTACHARYYA P. Repeatability and stability of room temperature acetone sensor based on TiO_2 nanotubes: Influence of stoichiometry variation [J]. IEEE Transactions on Device and Materials Reliability, 2014, 14: 961−967.

[42] WANG Yu-de, CHEN Jing-bo, WU Xing-hui. Preparation and gas sensing properties of perovskite type $SrFeO_3$ oxide [J]. Materials Letters 2001, 49: 361−364.

[43] XIAO Yuan-hua, LU Ling-zhen, ZHANG Ai-qin, ZHANG Yong-hui, SUN Li, HUO Lei, LI Feng. Highly enhanced acetone sensing performances of porous and single crystalline ZnO nanosheets: High percentage of exposed (100) facets working together with surface modification with Pd nanoparticles [J]. ACS Applied Materials & Interfaces, 2012, 4: 3797−3804.

[44] WANG Cheng-xiang, YIN Long-wei, ZHANG Lu-yuan, XIANG Dong, GAO Rui. Metal oxide gas sensors: Sensitivity and influencing factors [J]. Sensors, 2010, 10: 2088−2106.

[45] RENITTA A, VIJAYALAKSHMI K A. Novel room temperature ethanol sensor based on catalytic Fe activated porous WO_3 microspheres [J]. Catalysis Communications, 2016, 73: 58−62.

[46] ROY S, BANERJEE N, SARKAR C K, BHATTACHARYYA P. Development of an ethanol sensor based on CBD grown ZnO nanorods [J]. Solid-State Electronics, 2013, 87: 43−50.

[47] ZHOU Lie-jing, LI Chun-guang, ZOU Xio-xin, ZHAO Jun, JIN Pan-pan, FENG Liang-liang, FAN Mei-hong, LI Guo-dong. Porous nanoplate-assembled CdO/ZnO composite microstructures: A highly sensitive material for ethanol detection [J]. Sensors and Actuators B, 2014, 197: 370−375.

基于新型形貌的纳米结构氧化锌高性能室温气体传感器

Naila ZUBAIR, Khalida AKHTAR

National Center of Excellence in Physical Chemistry, University of Peshawar,
Peshawar-25120, Khyber Pukhtoonkhwa, Pakistan

摘　要：通过简单快速且无添加剂的氨水可控沉淀法在水溶液中制备具有新型形貌和均匀纳米结构的氧化锌粉末。用 SEM、XRD、FTIR、TG/DTA 等检测手段表征所制备的固体粉末。FTIR 分析结果显示：纳米结构形貌对所制备材料的红外光谱影响较小。将原始态(ZnO-AP)、烧结态(ZnO-Cal)和商业(ZnO-Com)纳米结构 ZnO 制作成气敏元件，并在室温(29 °C)下检测其对氨气、丙酮和酒精的气敏性能。结果表明，ZnO-AP 和 ZnO-Cal 气敏元件对 1×10^{-6} 的氨气表现出优良的气敏性能和可重复性，灵敏度分别为 63.79% 和 66.87%，响应和恢复时间分别为 13 和 3 s；这是由于合成的纳米结构具有独特的形貌和优异的形状与尺寸均匀性。相反，ZnO-Com 气敏元件对浓度 200×10^{-6} 以下的氨气没有响应。另外，ZnO-Cal 在室温下对氨气的选择性高于对丙酮和酒精的选择性。总之，合成的 ZnO 对氨气的最低检测限为 1×10^{-6}，表明其具有优异的气敏特性。

关键词：氧化锌纳米结构；气体传感器；敏感性；响应/恢复时间

(Edited by Bing YANG)